Spalling uniaxial strength of Al_2O_3 at high strain rates

M.J. Pérez-Martín, B. Erice, D.A. Cendón, and F. Gálvez

Abstract. In this article research into the uniaxial tensile strength of Al_2O_3 monolithic ceramic is presented. The experimental procedure of the spalling of long bars is investigated from different approaches. This method is used to obtain the tensile strength at high strain rates under uniaxial conditions. Different methodologies proposed by several authors are used to obtain the tensile strength. The hypotheses needed for the experimental set-up are also checked, and the requirements of the set-up and the variables are also studied by means of numerical simulations. The research shows that the shape of the projectile is crucial to achieve successfully tests results. An experimental campaign has been carried out including high speed video and a digital image correlation system to obtain the tensile strength of alumina. Finally, a comparison of the test results provided by three different methods proposed by different authors is presented. The tensile strength obtained from the three such methods on the same specimens provides contrasting results. Mean values vary from one method to another but the trends are similar for two of the methods. The third method gives less scatter, though the mean values obtained are lower and do not follow the same trend as the other methods for the different specimens.

1 Introduction

Advanced ceramic materials are mostly used in armour systems, turbine blades and other structural elements, given their high strength level in dynamic loading conditions and at elevated temperatures. The main applications are in the field of ballistic armour, where the mechanical properties of such ceramics find themselves in an advantageous position when compared with other materials. As a basic description, these materials present a linear elastic behaviour up to fracture. However, some localised plasticity could appear at high temperatures or when the strain rate increases dramatically. The main properties are high stiffness and compressive strength. In some cases, the elastic modulus of these materials can reach twice the value of the steel. Nevertheless, one of the weakest points of such materials is the tensile strength, with it being one order of magnitude below the compressive strength.

In order to predict the failure of a ceramic component, its tensile strength should be obtained. It is well known that the tensile strength of the materials may vary with the strain rate. The evaluation of this factor is essential from the design point of view. However, the scientific community has not reached agreement about the most appropriate testing method to obtain the tensile strength of brittle materials at different strain rates. In addition, measuring the tensile strength ceramic materials is far from being an easy task.

With the aim of obtaining the tensile strength of advanced ceramics at high strain rates, many different testing procedures have been used. Nevertheless, some associated difficulties could be encountered when using such methods.

Carrying out tensile tests using Split Hopkinson Tension Bar (SHTB), is one of the procedures. The complex alignment of the loads during the experiments makes this method highly undesirable. Different specimen geometries have been designed for this purpose [1]. These geometries not only avoid complexity of the method, but they also make it quite expensive. An alternative method is to measure the flexure strength of beams [2], providing the modulus of rupture. This serves as a sound approximation to the problem, though it is not the actual tensile strength of the material.

The Brazilian or splitting tests of discs provide the researcher with a reliable alternative to the procedures mentioned above. Materials with compressive strength much higher than tensile strength are required to perform these Brazilian tests. It is assumed that ceramic materials behave in such this way. This procedure is widely extended in other materials such as concrete or rocks (Rocco et al. [3]). It has been successfully applied to advanced ceramics [4], not only in static tests but also under dynamic loading conditions. The splitting test in using a Split Hopkinson Pressure Bar (SHPB) [5] was introduced by Rodríguez et al. [6] as a method to measure the tensile strength in brittle materials. While it is a valid option to obtain the tensile strength, one of the main disadvantages lies in the local biaxial stress states that appear at the failure starting points. As stated by Gálvez et al. [7] using this procedure may lead to inaccurate measurements of the tensile strength.

Although spalling of rods has been investigated for some time [8,9] there have been few studies that make use of it quantitatively for measuring the tensile strength of brittle solids. Rather, in recent years spalling produced by explosive or plate-impact loading has been used for this purpose. These two types of loading produce quite different pulse shapes: explosive loading producing triangular-shaped pulses as opposed to rectangular pulses produced by plate impact. This is a problem if our interest is in, say, blast loading of materials used in structures as the spall mechanisms are very different [10–12]. The first discussion of spalling by triangular waves was by Taylor [13], picking up on studies performed by B. Hopkinson in 1914 [5]. Thus, spalling by shock pulses is sometimes termed 'Hopkinson fracture' and triangular shock pulses 'Taylor waves'.

The spalling of long bars has proved to be a successful method in obtaining the true tensile strength of brittle materials. Uniaxial stress states can be achieved using this procedure, but only under dynamic loading conditions. This technique is based on the elastic wave propagation in long bars first described by Najar et al. [14], Johnstone et al. [15] and Gálvez et al. [16,17]. The principles of the method are presented and studied in detail by Gálvez et al. [18]. This research proposes and validates a procedure to obtain the tensile strength of brittle materials. Summarising, the spalling test of long bars is a technique that provides the tensile strength of brittle materials at high strain rates under uniaxial stress conditions. This has been applied to several materials such as: alumina by Gálvez et al. [19], concrete by Diamaruya et al. [20], Klepaczko et al. [21], and Brara et al. [22]. And more recently to other materials such as reinforced concrete by Dong et al. [23] and GFRC by Govender et al. [24].

2 The fundamentals of the spalling of long bars

The procedure of the spalling test in long bars is based on the propagation of controlled compressive elastic stress waves and the reflection as tensile loads at a specimen free end. When applied to materials with a compressive strength much higher than the tensile strength, the capacity to support compressive loads without any damage combined with the tensile weakness, can lead to a controlled failure when tensile loads are generated. In order to ensure that the uniaxial elastic wave propagation theory can be applied, a large length over diameter ratio (long bar geometry) is needed.

The test procedure consists of the initiation of a compressive wave in a long bar ceramic specimen. The wave is generated using the same set-up of a Hopkinson bar in its compressive configuration, which is composed by a striker bar (projectile), an input bar and an output bar. The last one is in this case the specimen with one of its ends free. Typically the projectile, the input bar and the specimen have the same diameter. However, some authors such as Wu et al. [25] have used different diameter configurations. It is assumed that the projectile and the input bar behave as purely linear elastic material. Therefore, high yield stress steels serve as an appropriate choice for this purpose. The output bar is the brittle specimen, where the end which is not in contact with the input bar is a free boundary. The compressive wave generated by the impact of the projectile travels along the input bar and is transmitted to the specimen. This wave eventually reaches the free end where it is reflected as a tensile wave producing the failure of the material. The input bar or the specimen, or even both, are instrumented with strain gauges with the aim of measuring the incident and reflected pulses. Compressive loads generated in the test should not produce any damage in the specimen; otherwise incorrect measurements of the tensile strength may be obtained. On the other hand, the compressive wave must be high enough to ensure that the reflected one reaches the tensile strength of the specimen.

Therefore, the subsequent hypotheses are assumed:

- The test is only applicable to those materials having a compressive strength much higher than in tension.
- The specimen cannot be damaged during the initial transmitted compressive pulse.
- The material response of the specimen must remain linear elastic until failure occurs.
- The experimental set-up has to provide one-dimensional elastic wave propagation.

As an additional requirement, the pulse shape should make it possible to identify clearly the failure in a unique initial crack, even in the case of the later appearance of other secondary cracks. This could be achieved by modifying the shape of the projectile as proposed by Gálvez et al. [18]. The accomplishment of the hypotheses previously described is essential in obtaining the tensile strength with this procedure.

3 Methods for the tensile strength measurement

In order to analyse the test results and obtain the tensile strength of the material, different approaches can be followed. Gálvez et al. [18] proposed a method based on the measurement of the introduced compressive wave to the specimen, obtaining the reflection wave pattern. Klepaczko et al. [21] described another method, based on the velocity of the different fragments after the tensile failure of the specimen. Gómez del Río et al. [26] showed that the measurement of the pulse that overcomes the fracture point could be used to reconstruct its initial value using a dispersion correction method.

The method proposed by Gálvez et al. [18] is based on the calculation of the reflection wave on the free end of the specimen. This method has been followed by Wu et al [25] and Erzar et al. [27] and has provided successful results. According to Gálvez et al. [18], the reflection of the compressive wave at the free end of the specimen produces a growing reflected tensile pulse. This gives a maximum tensile stress at a defined location as a function of time. As explained by Gálvez et al. [18, 19], the tensile strength can be obtained by identifying the location of the first crack using high-speed image acquisition systems and correlating the maximum tensile value of the stress profile in the specimen. This provides the tensile strength of the specimen. The mean strain rate, $\dot{\varepsilon}_{spalling}$, reached in the spalling tests, was obtained from the stresses derived in the fracture plane with the following expression:

$$\dot{\varepsilon}_{spalling} = \frac{1}{E}\left(\frac{\partial \sigma}{\partial t}\right)_{FracturePlane}, \quad \sigma > 0 \tag{1}$$

where E is the elastic modulus of the specimen, σ is the stress and t the time.

The method proposed by Klepaczko et al. [21] is based on the measurements of the ejection velocity of the different specimen fragments after specimen failure. They report that the tensile strength, σ_F, can be measured by the following expressions:

$$\sigma_F = \rho C_0 v_e, \quad v_e = \frac{\Delta z\,(t_i) - \Delta z\,(t_{i-1})}{t_i - t_{i-1}} \tag{2}$$

where v_e is the called ejection velocity, $\Delta z(t_i)$ is the distance between fragments at the instant t_i where sub index i corresponds to the different images taken with high-speed image acquisition system, ρ is the specimen density and C_0 is the elastic wave propagation velocity. For this purpose a high speed camera to track the different fragments on concrete specimens is used on their experiments.

The analysis by Gómez del Río et al. [26] is based on the wave reconstruction of the tensile pulse measured behind the specimen failure location. On instrumented specimens, the strain gauge measures the incident pulse, and after failure occurs, also measures the tensile wave that has surpassed the fracture crack, the residual tensile pulse. If the strain gauge were located close enough to the failure location, the maximum stress value of this pulse would be similar to the tensile strength (see Eq. (3)) of the specimen. The greater the distance between the initial crack and the strain gauge, the more attenuated is the residual pulse. It is possible to reconstruct the tensile stress at the fracture location point, by giving the maximum tensile stress at the fracture location point which is the tensile strength. The results of the authors reveal that the tensile strength σ_F could be computed as:

$$\sigma_F = \sigma_m + A\,(z_f - z_g) \tag{3}$$

where z_f and z_g are the locations of the gauge and the failure point, σ_m is the maximum tensile stress of the residual pulse and A is the attenuation, a material constant.

4 Numerical simulations

As described above, to obtain the tensile strength using the methods seen in the previous section, it is necessary to obtain a unique initial crack. A clearly identified maximum on the tensile stress pulse is necessary to obtain such a crack. This

maximum increases while it travels along the specimen. This leads to a relationship between the maximum stress and its location, making it possible to identify the maximum value of the tensile load at the fracture point. As stated by Gálvez et al. [18], one of the most reliable methods to achieve this behaviour on the reflection of the waves is to have an incident pulse with a triangular shape with different raising and decreasing slopes. One of the possibilities to obtain this compressive pulse is to modify the geometry of the projectile. In order to have a proper contact between bars, many aspects such as bar alignment and condition (cleanness and roughness, among others) of the surfaces in contact have to be taken into account. The raising slope depends on the contact between the projectile and the input bar. To control the rising slope in these kinds of experiments is challenging. The decreasing slope of the pulse is due to the reflection of the wave on the end of the projectile not being in contact with the input bar. When the geometry of the projectile is symmetric, the pulse is also symmetric. Hence, the easiest way to control the decreasing slope of this pulse is modifying the geometry of this end of the projectile. A conical frustum geometry is proposed for the end of the projectile.

In order to know the influence of the proposed projectile geometry in the incident pulse shape, full 3D numerical simulations of the impact between projectile and input bars were carried out. To perform the numerical simulations LS-DYNA non-linear finite element code was used.

The projectile length was set to $L_p = 25\,\text{mm}$ and its diameter to $D = 8$ mm. This choice is explained in detail in the next section. The geometrical variables studied with the numerical simulations are the conical frustum length (ℓ) and its lower diameter (d).

Both projectile and input bar were made of steel. The steel was modelled using MAT_ELASTIC with the density $\rho = 7850\ \text{Kg/m}^3$, elastic modulus $E = 210$ GPa and Poisson's ratio $\nu = 0.3$. The contact between parts was modelled with the penalty formulation available in LS-DYNA, using AUTOMATIC_SINGLE_SURFACE command. Five different numerical simulations using a cylindrical ($\ell = 0\,\text{mm}$, $d = 8\,\text{mm}$), projectile varying the element sizes from $1.0 \times 1.0\,\text{mm}^2$ to $0.167 \times 0.167\,\text{mm}^2$, were performed to ensure that there was no influence of the mesh. Obviously, in order to reduce the computation time, the element size chosen was the coarsest one ($1.0 \times 1.0\,\text{mm}^2$).

Two sets of simulations were performed: in the first one, the lower diameter (d) was set to 2 mm varying the conical frustum length (ℓ) between 0 and 20 mm; in the second one, the conical frustum length (ℓ) was set to 20 mm varying the lower diameter (d) between 2 and 8 mm. Stress measures were taken in the middle of the input bar, the location of the strain gauges in the experimental set-up. Good agreement between numerical simulations and experimental data (see Sect. 5) using a cylindrical projectile, as can be seen in Fig. 1, was obtained. Figure 1(a) also shows that increasing the conical frustum length changes the shape of the compressive incident wave into a triangle-like form. The same effect occurs when decreasing the lower diameter (see Fig. 1(b)). In accordance with such simulations, a projectile with $\ell = 20\,\text{mm}$ and $d = 4\,\text{mm}$ was selected and manufactured. Note that the most triangular shape would be achieved by using $d = 2\,\text{mm}$: however, and unfortunately, it was not possible to manufacture it properly.

The effect of a possible misalignment when impact occurs was assessed using the final geometry of the projectile. Numerical simulations varying the misalignment angle between 0.5° and 5° were carried out. As can be seen in Fig. 2(a), a maximum misalignment of 5° can cause up to 5% difference between upper and lower values of stresses on the cross-section area. Note that Fig. 2(b) represents the cross-section area at the middle of the input bar.

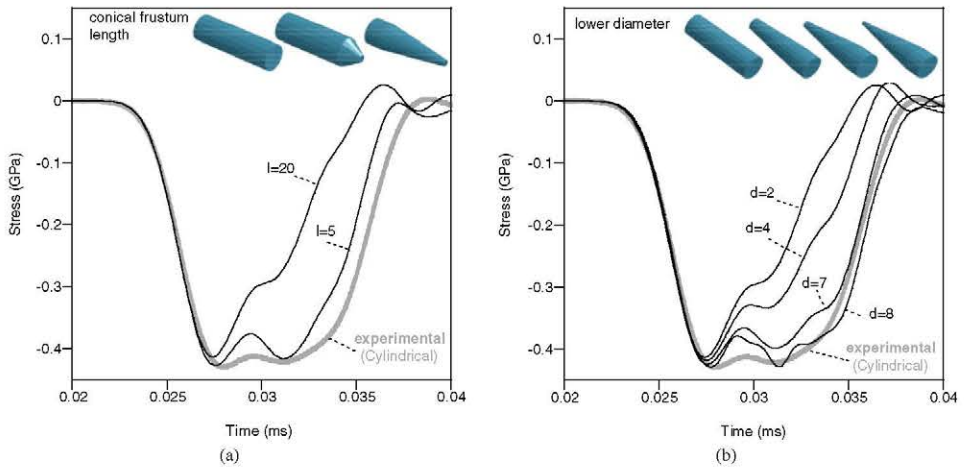

Fig. 1. Incident wave as a function of the projectile geometry using numerical simulations. (a) Conical frustum length influence using a fixed lower diameter of 2mm. (b) Lower diameter influence using a fixed 20 mm conical frustum length.

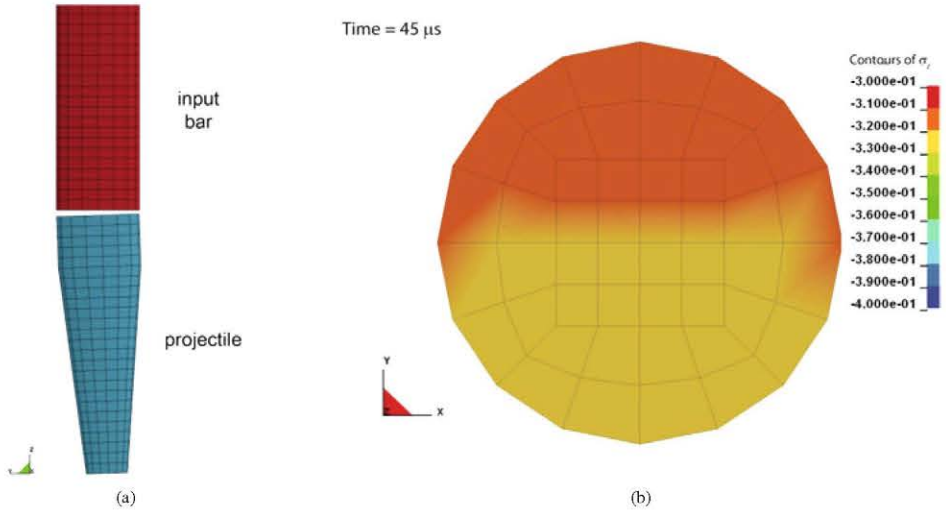

Fig. 2. (a) Misalignment between projectile and input bar. (b) Contours of the axial stress on the input bar for a 5° misaligned impact.

5 Experiments

The material tested in this research was a high purity alumina which behaves elastically up to failure with a compressive strength about an order of magnitude higher than the tensile strength. The material was a 99.5% purity alumina supplied by Morgan Advanced Ceramics.

The specimens are cylinders of 100 mm long and 8 mm diameter, the same geometry used by Gálvez et al. [18] and Gómez del Río et al. [26]. All specimens had been carefully measured, weighted and inspected. To obtain the elastic properties the impulse excitation technique with a Grindosonic MK equipment was used. The measurements are summarised in Table 1. In addition, all the specimens were instrumented with two strain gauges at 80 mm of the free end in opposite sides of a diameter

Table 1. Geometry, density and elastic properties for 99.5% purity alumina.

Specimen ID	Length (mm)	Diameter (mm)	Density (kg/m^3)	Poisson's Ratio	Elastic modulus (GPa)
R01	100.03	7.99	3876	0.23	373.4
R02	100.05	8.00	3860	0.23	370.8
R03	100.02	7.99	3880	0.23	374.2
R04	99.99	7.99	3874	0.23	372.3
R05	100.03	7.98	3887	0.23	375.7
R06	100.01	8.00	3871	0.23	372.4
R07	100.04	7.99	3872	0.23	372.8
R08	100.02	8.00	3866	0.23	371.4
R09	100.01	8.00	3873	0.23	372.3

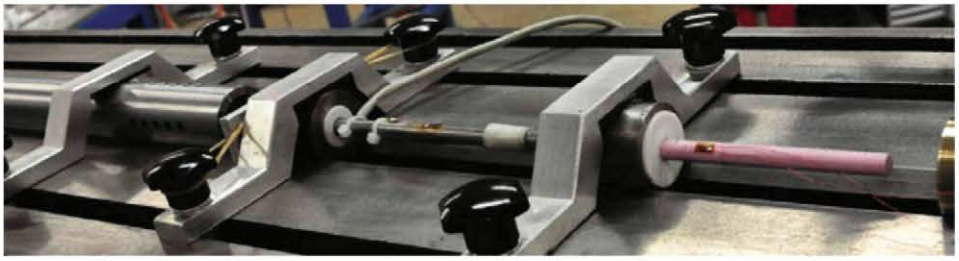

Fig. 3. Experimental set-up showing the barrel, the incident bar, the instrumented specimen and the fragment recovery system. All items mounted over a V-shape bedplate.

to measure the initial compressive wave applied. A speckle pattern was painted on the specimens in order to perform a Digital Image Correlation (DIC) analysis of the images taken during the tests.

The diameter of the projectile was chosen as 8 mm in order to maintain the same diameter as in the input bar and specimen. For optimal data acquisition, a proper design of the projectile was necessary. The time t that takes a one-dimensional wave to travel along a distance L on an elastic solid was:

$$t = L/C \tag{4}$$

where C is the elastic wave propagation velocity. According to Eq. (4) the compressive pulse length t_p is ruled by the length of the projectile L_p with $t_p = 2L_p/C_p$, which is the time the wave takes to travel back and forth inside the projectile, with C_p being the elastic wave propagation velocity in the projectile. Having fixed the length of the specimen L_s, to avoid overlapping between incident and reflected waves, the length of the projectile must not be longer than:

$$L_p = \frac{1}{2} L_s \frac{C_p}{C_s} \tag{5}$$

where C_s is the elastic wave propagation velocity in the specimen. In this particular case C_p= 5150 m/s, C_s= 9800 m/s and $L_s = 100$ mm, which leads to a final projectile length of $L_p \simeq 1/4 L_s = 25$ mm.

The experimental set-up (see Fig. 3), consisted of a steel frame in which a "V" shape hollow machined to ensure proper alignment of the system. The gas cannon was 600 mm long and the input bar 200 mm long and 8 mm in diameter. A residual fragment collector device was included close to the free end of the specimen. All the

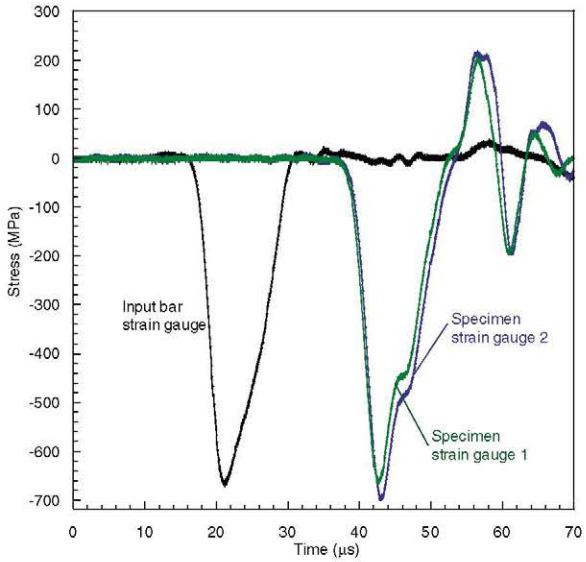

Fig. 4. Strain gauge recordings of the input bar and the specimen.

tests were recorded using a v12 Phantom high speed camera. The high speed camera was set up to record 150.134 frames per second, taking 512×64 pixels resolution images with $6.66\,\mu$s spacing between each one.

To avoid damage on the specimen due to the initial compressive wave, a previous compression test was carried out. This last test was performed adding a second bar (output bar) immediately after the specimen. The bar was in contact with the specimen, sandwiched between the two steel bars (input and output). This method enabled the inclusion of a compressive wave identical to the one expected in the spalling test, though avoiding the reflection on the free end of the specimen as tensile wave. After this compression test, no damage was found on the specimens. A measure of the dynamic elastic modulus before and after compression test allowed for verification that there was no trace of damage on the samples.

6 Results

All the specimens tested were analysed following the three methods mentioned in Sect. 3. The wave recordings for the input bar and for the specimens showed, as expected (see Fig. 4), a triangular shape. In Fig. 5 four pictures taken during the spalling tests are shown which helped to reveal the cracks.

Following the method performed by Gálvez et al. [18], the wave reflection gives a tensile maximum value as a function of time, and so as a function of the position on the specimen shown in Fig. 6(a). This method provides the tensile strength of the material by identifying the fracture location and taking into account the stress state at this time. The results for all the specimens tested are plotted in Fig. 6(b). The values obtained show a large scatter, though this is typical for the material tested and should not be related to the testing method.

The second method evaluated was that proposed by Klepaczko et al. [21]. This method above described (see Sect. 3) is based on the velocity of the different fragments after the tensile failure of the specimen. In order to obtain these velocities, the images recorded from the high speed camera were post-processed and analysed with DIC

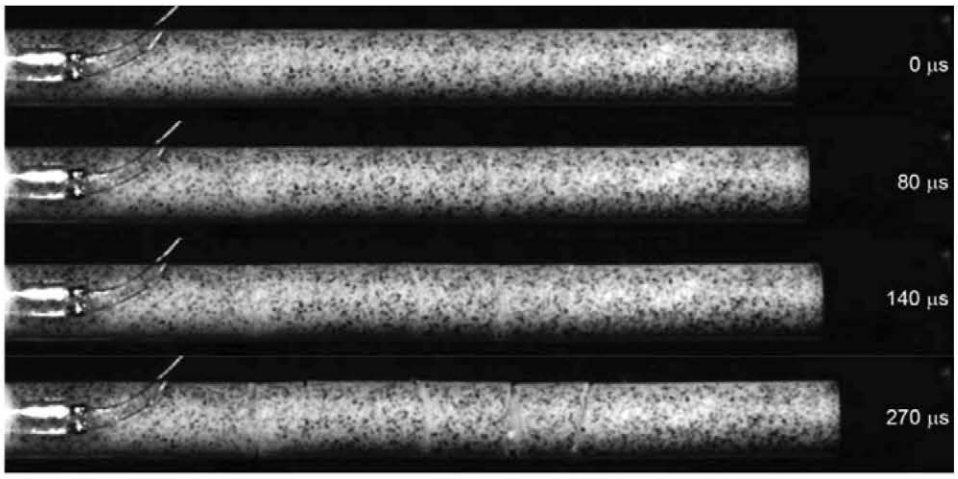

Fig. 5. Pictures taken from the spalling test with specimen ID R09 showing the locations of the cracks.

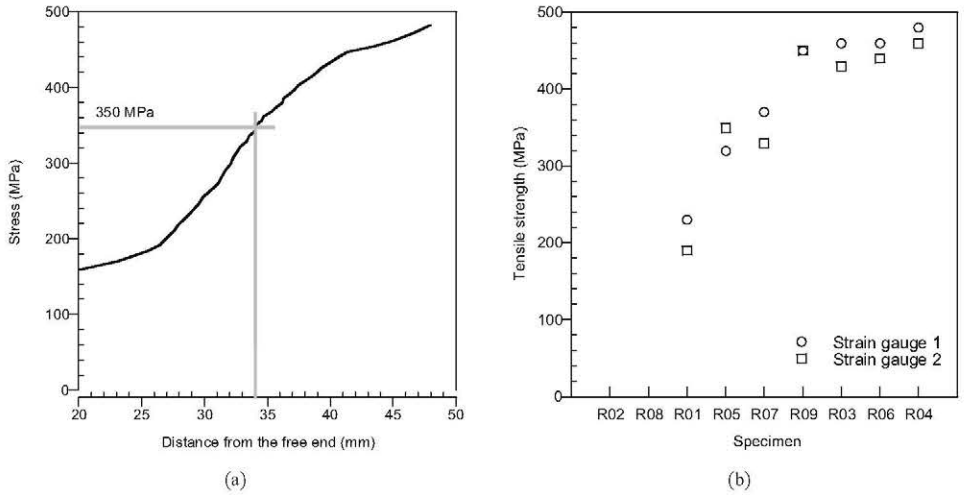

Fig. 6. Measurement of the tensile strength using the method proposed by Galvez et al. [18] On the left (a), the method used and on the right (b) the results obtained for the different specimens tested.

software. Furthermore, this DIC system allowed location of the different cracks in the specimen. The velocity measurements obtained with DIC software can be seen in Fig. 7. The observation of the high speed videos and the results revealed that the first crack is of a higher value of the tensile strength. The tensile strength obtained using this method is shown in Fig. 8(a).

The third method evaluated is that proposed by Gómez del Río et al. [26] described in detail in Sect. 3. Knowing the position of the first crack, the residual tensile pulse and attenuation value, in this case 10 MPa/μs, the tensile strength was calculated for all the specimens. The results of the tensile strength using this method are plotted in Fig. 8(b).

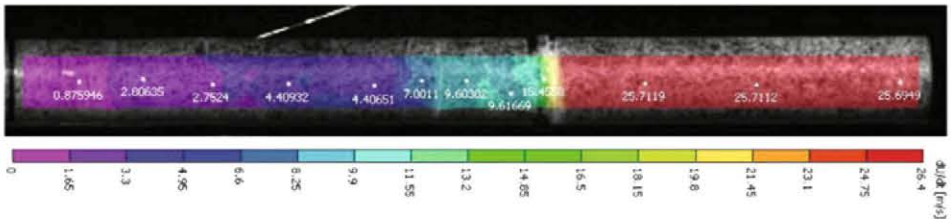

Fig. 7. Velocity measurements of the different fragments using the DIC software.

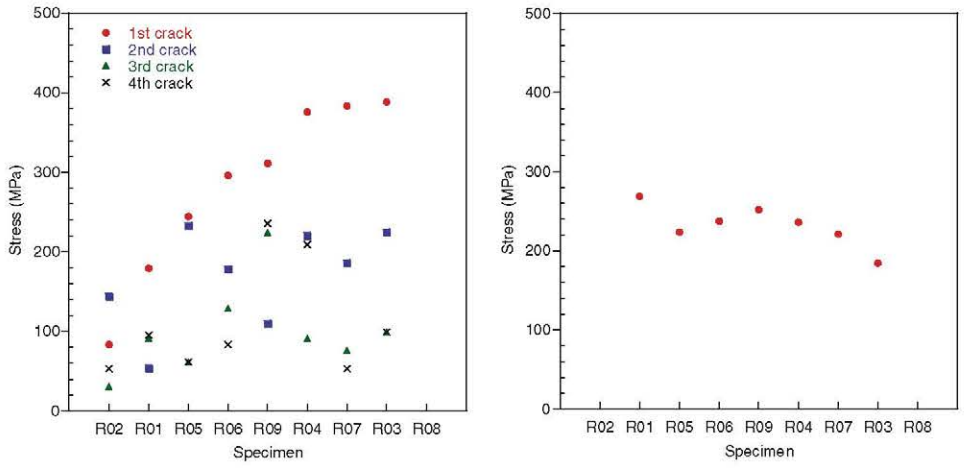

(a) (b)

Fig. 8. (a) Tensile strength obtained using the method proposed by Klepaczko et al. [21] for several cracks in order of appearance. (b) Tensile strength obtained using the method proposed by Gómez del Río et al. [26] for the first crack.

7 Discussion

For the method proposed by Gálvez [18], the instrumentation of the specimens is necessary. The measurements on the incident bar are not valid for the wave reflection analysis, even when correcting the wave using the impedances on both materials. The wave changes its shape enough to give poor results due to the quality of bar-specimen contact. This can be observed in Fig. 4, where the incident compressive wave is not exactly the wave measured on the specimen. Measurements in two different strain gauges on the specimen give the same wave shape, though there are some differences on the maximum value. This can be explained by a misalignment of the projectile-bar contact or in the bar-specimen contact. For that reason, a mean value obtained from both gauge measurements was selected for the tensile strength. The method is consistent and allows for easy calculation of the tensile strength using a small piece of numerical code, needed to analyse the waves.

The method proposed by Klepaczko [21] is capable of giving a tensile strength measurement for all the cracks of the specimen. Nevertheless, only the first crack that appeared was taken into account to obtain the tensile strength. This is because during subsequent cracking some fragments may have interacted with others, leading to inaccurate values of the velocity. Due to the fast velocity changes during the experiments, high frame rate was required in the recordings.

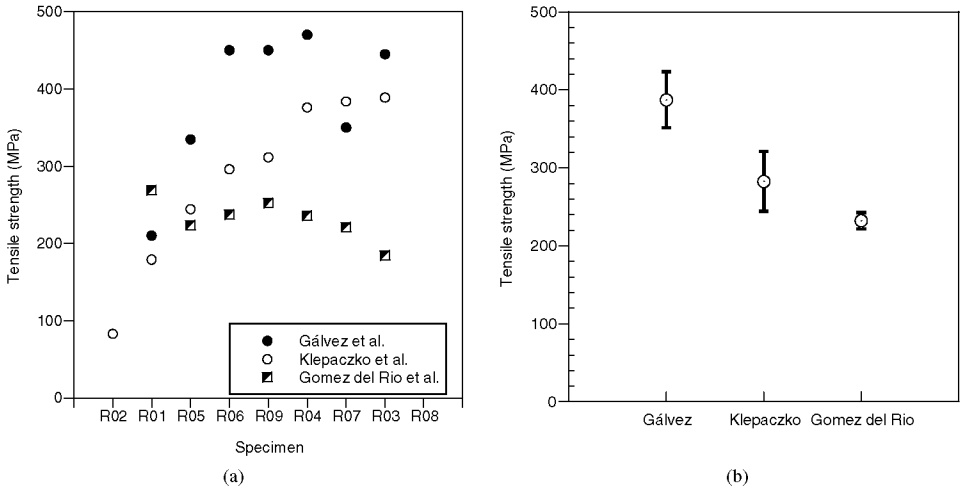

Fig. 9. Tensile strength measured using the three methods. (a) all the specimens; (b) mean value and its standard deviation.

The method proposed by Gómez del Río [26] was found to provide lower values for the tensile strength. One explanation for this effect is that there could be secondary cracks appearing between the main failure point and the measurement point, suggesting that this method would give the minimum value for several failure points.

The three methods provide different results of the tensile strength (see Fig. 9(a)). Whereas the method proposed by Gálvez [18] gives the higher values, that of Gómez del Río [26] offers lower measurements, with the method provided by Klepaczko [21] being at a midpoint. The scatter revealed by the methods of Gálvez [18] and Klepaczko [21] are quite similar (as shown in 7b), though significantly lower when using those of Gómez del Río [26].

The authors would like to acknowledge the financial support through the project with reference BIA2011-24445 of the Spanish Ministry of Science and Innovation.

References

1. G.D. Quinn, Engineered Materials Handbook, Ceramic and Glasses, vol. 4 (ASM International, 1991)
2. G. Quinn, J. Amer. Ceram. Society **73**, 2374 (1990)
3. C. Rocco, G.V. Guinea, J. Planas, M. Elices, Mater. Struct. **32**, 210 (1999)
4. J.E.O. Ovri, T.J. Davies, Mater. Sci. Eng. **96**, 109 (1987)
5. B. Hopkinson, Philosophical Transactions of the Royal Society of London Series a – Containing Papers of a Mathematical or Physical Character **213**, 437 (1914)
6. J. Rodríguez, C. Navarro, V. Sanchez-Gálvez, J. Phys. IV (France) **4**, 101 (1994)
7. F. Gálvez, V. Sánchez-Galvez, J. Phys. IV (France) **110**, 347 (2003)
8. H. Kolsky, A.C. Shearman, Research **2**, 384 (1949)
9. H. Kolsky, Y.Y. Shi, Proc. Phys. Society London **72**, 447 (1958)
10. J.N. Johnson, J. Appl. Phys. **52**, 2812 (1981)
11. G.T. Gray, N.K. Bourne, B.L. Henrie, J.C.F. Millett, J. Phys. IV (France) **110**, 773 (2003)
12. S.A. Maloy, G.T. Gray, C.M. Cady, R.W. Rutherford, R.S. Hixson, Metall. Mater. Trans. a-Phys. Metall. Mater. Sci. **35A**, 2617 (2004)

13. G.I. Taylor, Research **5**, 508 (1952)
14. J. Najar, J. Phys. IV (France) **4**, 647 (1994)
15. C. Johnstone, C. Ruiz, Int. J. Solids Struct. **32**, 2647 (1995)
16. F. Gálvez, J. Rodríguez, V. Sánchez-Gálvez, J. Phys. IV (France) **07**, C3 (1997)
17. F. Gálvez, J. Rodríguez, V. Sánchez-Gálvez, J. Phys. IV (France) **10**, 203 (2000)
18. F. Gálvez Dìaz-Rubio, J. Rodrıguez Pérez, V. Sánchez-Gálvez, Int. J. Impact Eng. **27**, 161 (2002)
19. F. Gálvez, J. Rodríguez, V. Sánchez-Gálvez, J. Phys. IV (France) **10**, 323 (2000)
20. M. Diamaruya, H. Kobayashi, T. Nonaka, J. Phys. IV (France) **7**, 253 (1997)
21. J.R. Klepaczko, A. Brara, Int. J. Impact Eng. **25**, 387 (2001)
22. A. Brara, F. Camborde, J.R. Klepaczko, C. Mariotti, Mech. Mater. **33**, 33 (2001)
23. X.L. Dong, Z.Q. Hong, S.L. Zhang, J.Y. Chen, L. Wang, DYMAT 2009, 449 (EDP Sciences, 2009)
24. R. Govender, L. Louca, A. Pullen, G. Nurick, DYMAT 2009, 633 (EDP Sciences, 2009)
25. H.J. Wu, Q.M. Zhang, F.L. Huang, Q.K. Jin, Int. J. Impact Eng. **32**, 605 (2005)
26. T. Gómez del Río, J. Rodríguez Pérez, Int. J. Impact Eng. **34**, 377 (2007)
27. B. Erzar, P. Forquin, Exper. Mech. **50**, 941 (2010)